Available online at www.sciencedirect.com
ScienceDirect
Trans. Nonferrous Met. Soc. China 30(2020) 449−462
Transactions of Nonferrous Metals Society of China
www.tnmsc.cn

Evaluation of microstructure and texture formation during annealing of cold-rolled FeCrCuMnNi multiphase high-entropy alloy

Ali SHABANI, Mohammad Reza TOROGHINEJAD

Department of Materials Engineering, Isfahan University of Technology, Isfahan 84156-83111, Iran

Received 17 April 2019; accepted 31 July 2019

Abstract: Microstructure and texture variations of a cold-rolled multiphase FeCrCuMnNi high-entropy alloy were studied after different annealing treatments. Samples were heat-treated at different temperatures and for different time, and then, subjected to different tests including XRD and SEM-EBSD. The results reveal that the FCC1 phase, which goes through more strain, has lower melting temperature, and recrystallizes earlier (lower temperature and shorter time). In addition, it is seen that particle stimulated nucleation is more effective on the recrystallization of this phase compared to FCC2 phase. A significant number of FCC1 nuclei form around the BCC particles. Nucleation of FCC2 phase initiated at 800 °C mostly at the grain boundaries and the inhomogeneities. The FCC1 phase was almost fully recrystallized at this temperature. The annealing process led to the elimination of rolling textures, while the Brass component remained a major component in the recrystallized samples. Increasing annealing temperature as well as annealing time led to the formation of Cube texture component, which is a major component of recrystallized low stacking fault energy materials. Furthermore, D and Rt-Co components formed during recrystallization as a result of the formation of annealing twins.

Key words: high-entropy alloys; FeCrCuMnNi; recrystallization; microstructure; texture

1 Introduction

High-entropy alloys (HEAs) are equiatomic or near equiatomic multi-component materials consisting of five or more principal elements [1,2]. HEAs mostly tend to form simple solid solution structures such as face-centered cubic (FCC) phase, body-centered cubic (BCC) phase, hexagonal closed-packed (HCP), or a mixture of these phases rather than more complex intermetallic compounds. This may be due to their high mixing entropy [3−5]. Generally, HEAs possess efficient properties such as high thermal stability [6], superior tensile or compressive strength [7], extremely high hardness [8], and excellent corrosion resistance [9].

These properties are closely related to the structure and microstructure of HEAs, which can be manipulated through various methods including thermo-mechanical processing (TMP) [10−14]. TMP consists of heavy deformation and annealing, and often results in significant variation in microstructure and development of crystallographic texture through recrystallization [10,12,15,16]. Therefore, the microstructure evolution and texture variation during TMP seem to be essential, and have been studied widely in different materials [17−19]. Although researchers have recently tried to investigate these aspects of HEAs [13,16,20−22], more in-depth studies on microstructure and texture variation during TMP seem necessary.

Grain growth during annealing of HEAs has been reported as sluggish [13,16,23,24]. Solution hardening, low stacking fault energy, and sluggish diffusion have been reported as the main reasons for this phenomenon [13,16,20,25]. Some recent studies have also shown delayed recrystallization in HEAs compared to the traditional alloys [10,25,26].

Corresponding author: Ali SHABANI; E-mail: Ali.shabani@ma.iut.ac.ir
DOI: 10.1016/S1003-6326(20)65225-6

According to BHATTACHARJEE et al [27], dislocation energy and grain boundary energy decline due to the strain energy related to severe lattice distortion in HEAs; therefore, the driving force for recrystallization decreases. Furthermore, it has been revealed that the origin of annealing texture is strongly influenced by deformation texture, which depends upon the stacking fault energy (SFE) of HEAs [15]. In addition, it was reported that various processing parameters, such as strain, grain size, and strain path, can affect the recrystallization texture formation [28].

SATHIARAJ and BHATTACHARJEE [16] asserted that recrystallization texture is characterized by the retention of deformation texture components at lower annealing temperatures. They argued that increasing annealing temperature leads to grain growth, and consequently, changes in texture components. Additionally, in a recent study, ZHANG et al [22] stated that increasing annealing time could lead to a more uniform recrystallized texture. Nevertheless, further studies in these fields seem necessary due to the different alloying systems of HEAs. In addition, very few researches [13,20] have been published on the recrystallization of multiphase HEAs, which emphasize the importance of the present study. Single-phased HEAs have been found to reach a reasonable balance between strength and (tensile) ductility with difficulty. Therefore, a mixture of these phases could lead to an efficient balance between hardness and ductility [20,29]. FeCrCu-MnNi was reported as a multi-phase HEA with efficient mechanical properties in as cast and wrought conditions [29,30].

The objective of the present work was to study the evolution of microstructure and texture in FeCrCuMnNi alloy after cold-rolling and annealing heat treatments, which has so far not been reported. Therefore, phase stability, and microstructure and texture formation in the FeCrCuMnNi alloy were studied using X-ray diffraction (XRD) and scanning electron microscope-electron backscatter diffraction (SEM-EBSD) after the implementation of different annealing temperatures and times.

2 Experimental

The FeCrCuMnNi high-entropy alloy was produced through the vacuum induction melting (VIM) of high purity (>99.85%) raw materials. The raw materials were cleaned with acetone and dried before being charged into the crucible. Then, the chamber was brought to a vacuum of 1×10^{-3} Pa, and then, filled with high purity argon to 101.325 kPa. The vacuum-filling cycle was performed 2 times. The alloy was then cast into a graphite mold with the dimensions of 15 mm × 100 mm × 100 mm. To ensure the compositional homogeneity, the ingots were melted 2 times. Specimens with dimensions of 100 mm × 10 mm × 3 mm were cut from the as-cast sample, and heat-treated at 1000 °C for 4 h. Subsequently, the samples were cold-rolled to 85% thickness reduction. The cold-rolled samples were annealed at temperatures of 600, 700, 800, 900 and 1000 °C for 60 min to evaluate the effects of annealing temperature. In addition, other samples were annealed for 5, 30, 60, and 120 min at the temperature of 900 °C in order to investigate the effects of annealing time.

The probable variation of the crystal structure was investigated using a PHILIPS X-ray diffractometer with Cu K_α (λ=0.15406 nm) diffraction generated at 40 kV and 30 mA. The microstructure and texture of the samples were characterized using an EBSD system attached to a SEM (PHILIPS FEI XLF30) equipped with a field emission gun (FEG) electron source. Scan step size of 0.1−0.5 μm was used for the annealed samples. The EBSD data were collected from rolling direction/normal direction (RD/ND) plane. The samples were ground using a 4000 grit SiC polishing paper, and then, polished using a vibrating polisher (Bühler VibroMet 2). The microstructure, texture, recrystallized fraction, grain size, and distribution of the samples were extracted from EBSD results.

Additionally, using an automatic hardness measurement machine (Q10A, Qness, GmbH, Salzburg, Austria), Vickers microhardness tests were performed on the cold-rolled sample under a load of 5 g for 10 s.

3 Results

3.1 Cold-rolled sample

Figure 1(a) reveals the XRD pattern of the cold-rolled sample after 85% reduction in thickness. It can be seen that the cold-rolled alloy consists of

three different phases, including 2 FCC and 1 BCC phases, and the lattice parameters of these phases are 3.67, 3.62, and 2.88 Å, respectively. The microstructure of the sample presents a highly deformed lamellar microstructure aligned along the rolling direction, where FCC phases seem to sustain most of the imposed strain before transferring it to the BCC phase and aligned along the deformation direction as shown in Fig. 1(b). In addition, Fig. 1(c) demonstrates the φ_2=0°, 15°, 45°, and 65° sections of the orientation distribution functions (ODFs) of the FCC phase after 85% thickness reduction. The important texture components for FCC HEAs are presented in Table 1. It can be seen that Brass ({110}⟨112⟩), Rotated Goss (Rt-G) ({110}⟨110⟩), and shear texture (S1) ({111}⟨110⟩) components are the major texture components in FCC phase after deformation. Moreover, the hardness values of FCC1, FCC2, and BCC phases in the alloy are 426, 444, and 767, respectively. The compositions of the three different phases are summarized in Table 2. BCC phase, which is the hardest phase, is rich in Cr and Fe, and FCC1, which is the softest phase, shows Cu enrichment. Furthermore, FCC2 phase is also rich in Fe and Ni. The volume fractions of the BCC and FCC phases were roughly calculated using the following equation [31]:

$$W_{\mathrm{P}}=\frac{P}{\sum P_i}\times 100\% \tag{1}$$

where W_{P} is the volume fraction of the phase, P is the total peak intensity of a given phase in the XRD pattern, i is the number of the phase, and $\sum P_i$ is the total peak intensity of all phases in the XRD pattern. The cold-rolled alloy consisted of almost 34%, 60% and 6% of FCC1, FCC2, and BCC phases, respectively.

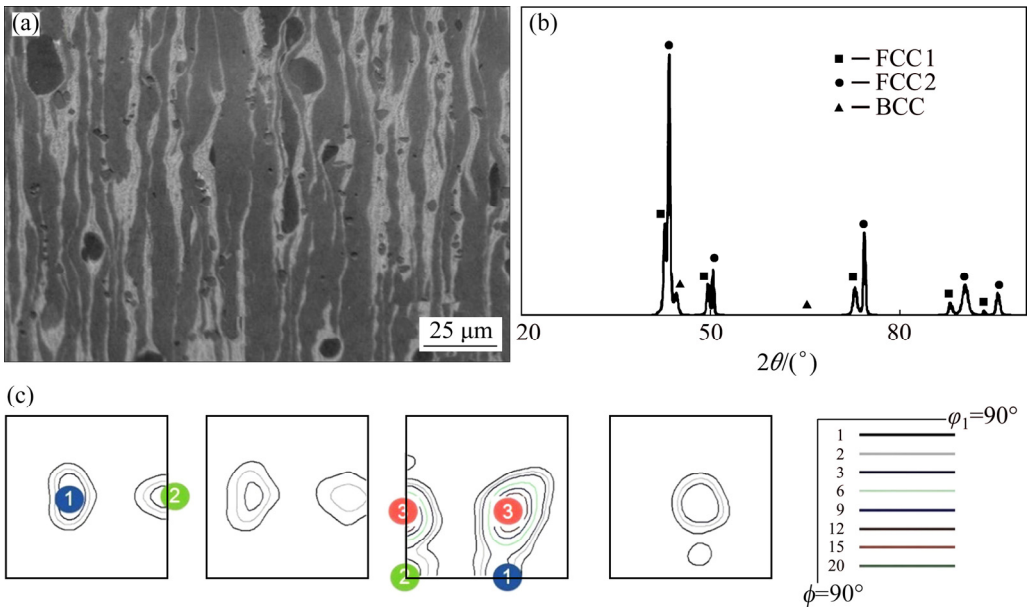

Fig. 1 85% cold-rolled sample characterization: (a) SEM image; (b) XRD pattern; (c) φ_2=0°, 15°, 45°, and 65° sections of ODF, respectively

Table 1 Important texture components in FCC HEAs

Texture component	Miller indices	φ_1/(°)	Φ/(°)	φ_2/(°)	Symbol
Brass	{110}⟨112⟩	35	45	0	1
Rotated Goss	{110}⟨110⟩	90	45	0	2
Shear texture (S1)	{111}⟨110⟩	0	55	45	3
Cube	{001}⟨100⟩	0	0	0	4
Dillamore	{4,4,11}⟨11,11,8⟩	90	27	45	5
Rotated copper	{112}⟨110⟩	0	35	45	6

Table 2 Chemical composition of cold-rolled sample and three phases of alloy (at.%)

Phase	Fe	Cr	Cu	Mn	Ni
Nominal	20	19.1	20.8	19.9	20.2
BCC	34.7	49.3	1.2	6.1	8.7
FCC1	6.5	3	53.7	19.6	17.2
FCC2	34.7	25	4.1	8.9	27.3

3.2 Structural and microstructural observations

Figures 2 and 3 illustrate the XRD patterns of the samples annealed for 60 min at different temperatures and at 900 °C for different time, respectively. It can be seen that in addition to the cold-rolled sample, annealed samples also consist of three different phases, including 2 FCC and 1 BCC phases. Furthermore, no phase transformation could be observed during annealing of the samples at different temperatures and for different time; however, variations in peak height could be the result of variation in the texture of the alloy due to the recrystallization process.

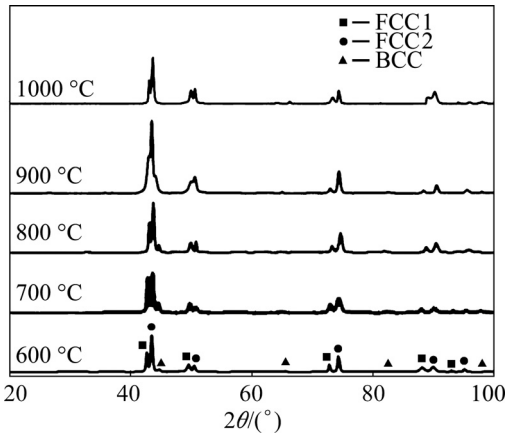

Fig. 2 XRD patterns of FeCrCuMnNi alloy annealed for 60 min at different temperatures

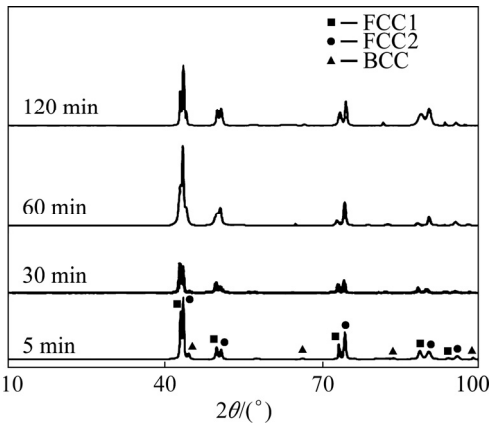

Fig. 3 XRD patterns of FeCrCuMnNi alloy annealed at 900 °C for different time

Figure 4 reveals the microstructure of the samples annealed at different temperatures. It can be seen that the recrystallization of the FCC1 phase, which is the softest phase, started at 600 °C as a result of the nucleation of new grains in the structure as shown by arrows in Fig. 4(a). However, recrystallized FCC2 phase was not observed at 600 °C. As illustrated in Fig. 5, less than 10% of the alloy recrystallized at this temperature. By increasing annealing temperature to 700 °C, nucleation and growth occurred in FCC1 and this phase seemed to reach complete recrystallization (see Fig. 4(b)). Furthermore, Fig. 5 illustrates that more than 30% of the alloy recrystallized at this temperature, which is almost the same amount as FCC1 phase. Nucleation of FCC2 phase started at 800 °C, while grain growth began in FCC1 phase at this temperature (Fig. 4(c)). However, the number of nuclei did not seem to be high and the recrystallized fraction increased less than 10% at this temperature. By increasing annealing temperature to 900 °C, grain growth proceeded in FCC1 phase and nucleation of a very high number of new recrystallized grains occurred in FCC2 phase as can be seen in Fig. 4(d). Recrystallized fraction increased to almost 70% at this temperature. Increasing the annealing temperature to 1000 °C resulted in a significant variation in the sample structure. As presented in Fig. 4(e), a fully recrystallized structure was achieved after annealing at 1000 °C. Moreover, grain growth led to coalescence of the FCC1 phase grains and formation of an almost continuous structure, and simultaneous spheroidization of the FCC2 phase grain in the matrix. Furthermore, Fig. 5 reveals that recrystallized fraction was enhanced to 100% at this temperature.

Figure 6 illustrates grain size distribution at different annealing temperatures. The large fraction of grains in the ultrafine range (less than 1 μm) at temperatures of 600 and 700 °C is due to the nucleation of new FCC1 grains. However, a large fraction of grains with diameters of less than 1 μm can also be seen at 800 °C (see Fig. 6(c)), which is a result of the formation of a large number of FCC2 nuclei at this temperature. As shown in Figs. 6(d) and (e), with increase in annealing temperature, the grain size distribution showed a more widespread range due to the grain growth in both phases.

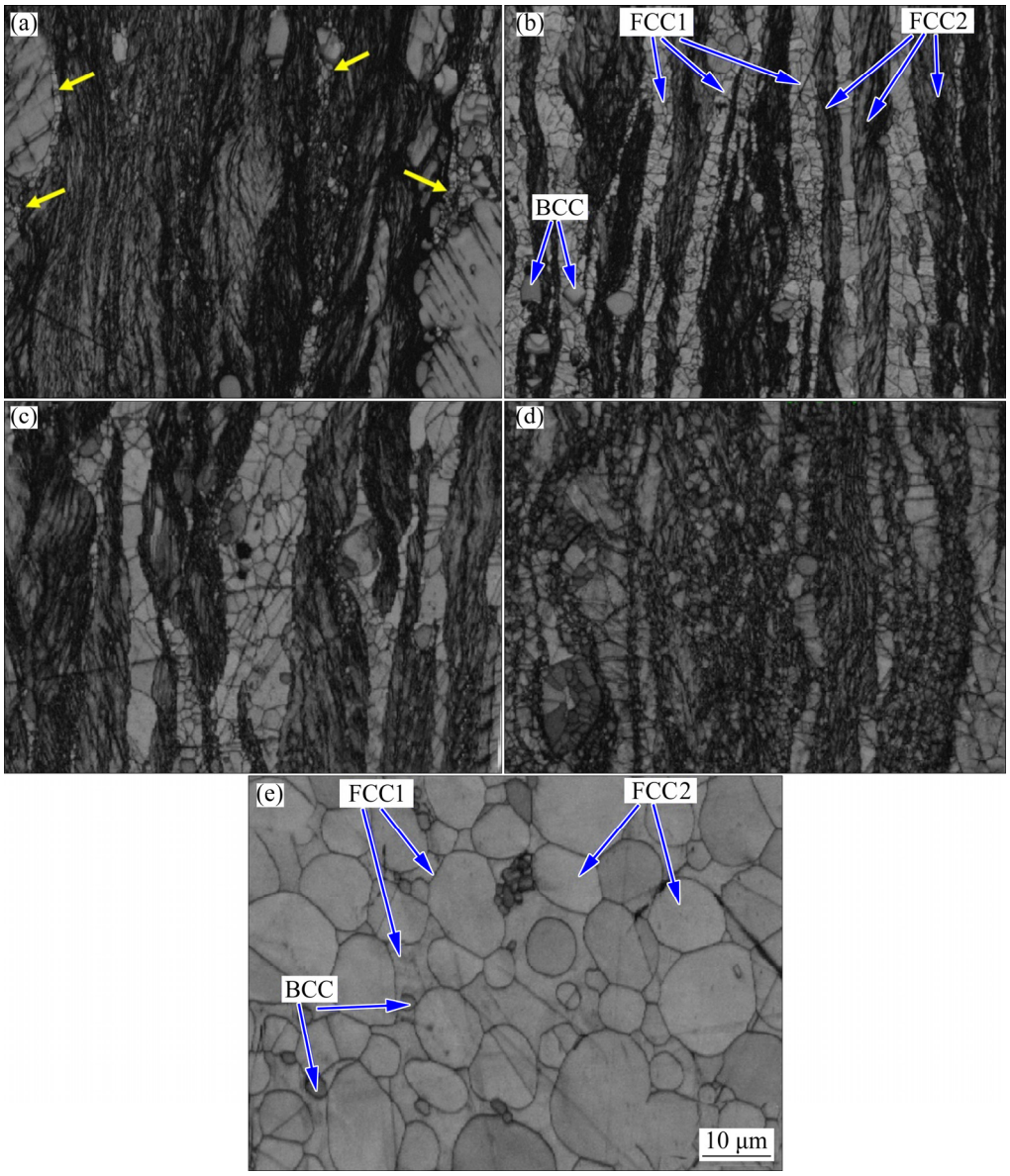

Fig. 4 SEM images of samples after 60 min of annealing at 600 °C (a), 700 °C (b), 800 °C (c), 900 °C (d), and 1000 °C (e)

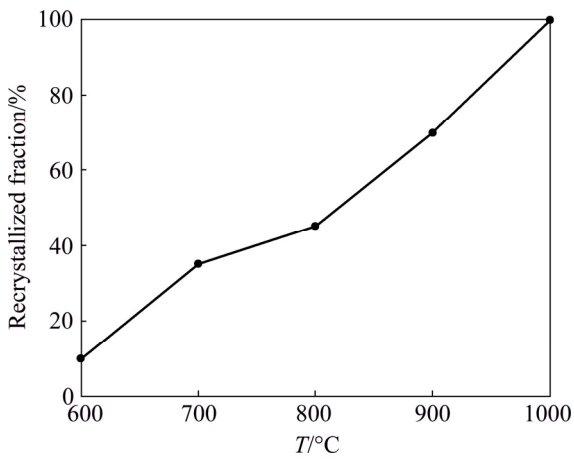

Fig. 5 Recrystallized fraction with increasing annealing temperature

Microstructure variation with increase in annealing time is shown in Fig. 7. It can be observed that FCC1 phase is fully recrystallized even after 5 min of annealing at 900 °C; however, a remarkable number of FCC2 phase nuclei can be observed. Therefore, as shown in Fig. 8, more than 40% of the alloy was recrystallized after 5 min of annealing at 900 °C. Increasing annealing time led to grain growth in both phases and nucleation of new grains in FCC2 phase. However, it seemed that grain growth proceeded slowly, as the recrystallized fractions increased to almost 60% and 70% after 30 and 60 min, respectively (see Fig. 8). Grain growth continued in both phases and an almost fully

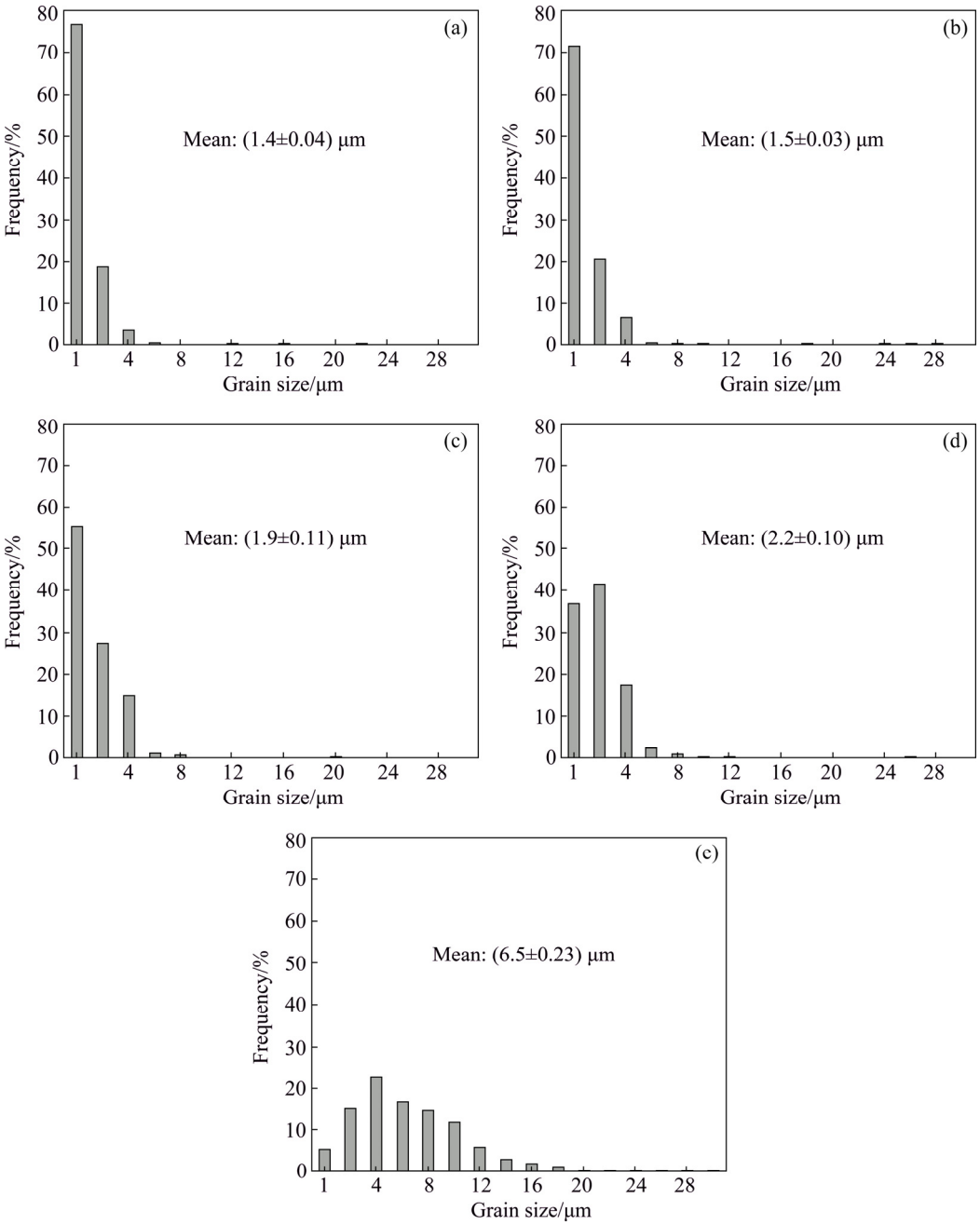

Fig. 6 Grain size distribution of samples after 60 min of annealing at 600 °C (a), 700 °C (b), 800 °C (c), 900 °C (d) and 1000 °C (e)

recrystallized microstructure (recrystallized fraction ~90%) was achieved after 120 min of annealing at 900 °C, as shown in Fig. 7(d).

Grain size distribution with increasing annealing time is presented in Fig. 9. A large fraction of grains with diameters of less than 1 μm can be seen in Figs. 9(a) and (b), which is due to the nucleation of FCC2 grains. Grain size distribution shows a more widespread range with increase in annealing time as grain growth occurs in both phases after 60 min of annealing at 900 °C. Grain size distribution shows a more widespread range with increase in annealing time as grain growth occurs in both phases after 60 and 120 min of annealing at 900 °C (see Figs. 9(c) and (d)).

3.3 Texture evaluation

Figure 10 demonstrates the φ_2=0°, 15°, 45°, and 65° sections of the ODFs of the FCC phase with increasing annealing temperature. The main texture components of the samples annealed at 600 °C are almost the same as that of the cold-rolled

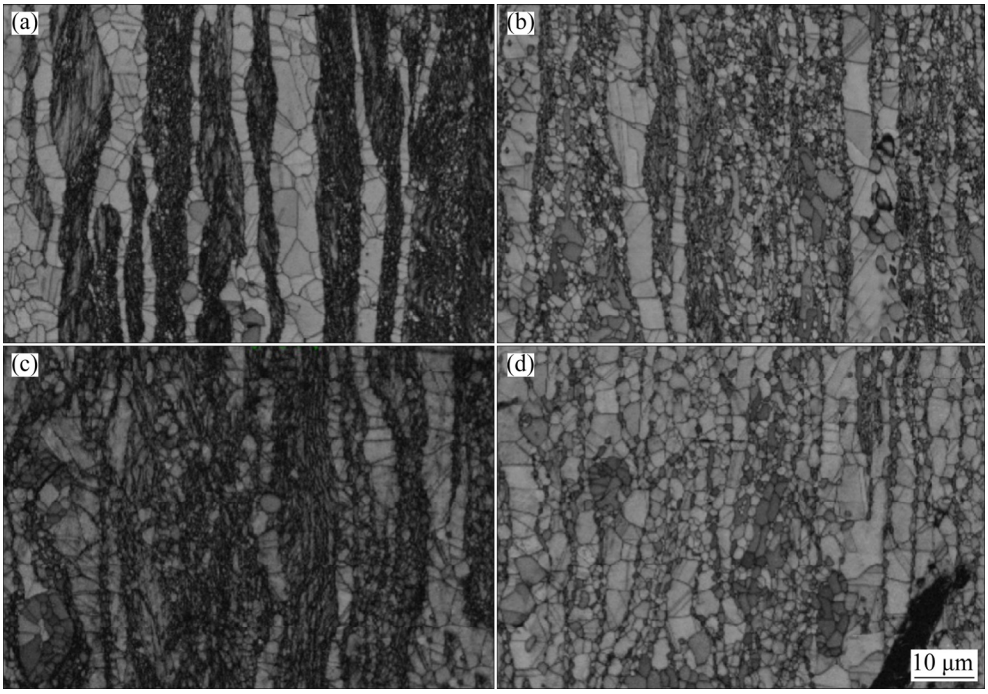

Fig. 7 SEM images of samples annealed at 900 °C for 5 min (a), 30 min (b), 60 min (c) and 120 min (d)

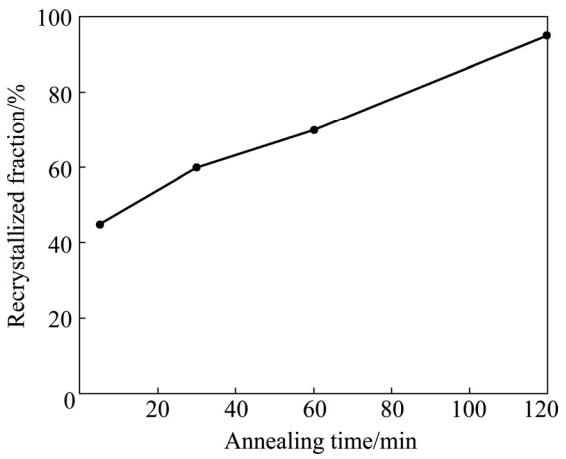

Fig. 8 Recrystallized fraction with increasing annealing time

samples. Brass, Rt-G, and S1 are the main texture components of these samples. Increasing annealing temperature to 700 °C led to a decrease in the intensity of the Brass and S1 components, whereas Rt-G remained almost stable. Figure 10(c) indicates completely different textural components in the sample annealed at 800 °C, which can be characterized as Cube ({001}⟨100⟩), Dillamore (D) ({4,4,11}⟨11,11,8⟩), and Rt-G. Increasing annealing temperature to 900 °C led to an intensity enhancement in the Cube and M components. At the same time, the Rt-G component weakened and the Brass component formed again. As shown in Fig. 10(e), in the sample annealed at 1000 °C, the Brass and D components were entirely eliminated and Cube and Rt-G weakened; however, a strong Rotated Copper (Rt-Co) ({112}⟨110⟩) component was formed.

In addition, changes in maximum intensity of major texture components with annealing temperature are presented in Table 3. The following points can be extracted from this table.

(1) Brass, Rt-G, and S1 are the main texture components in lower annealing temperatures.

(2) Increasing annealing temperature leads to a decrease in S1 (from almost 9×R to 0.2×R) and Rt-G (from almost 9×R to 4×R) intensity, but an increase in Cube and D intensity. Brass component reveals a swinging behavior; however, an increase was observed in Brass due to the increased temperature.

(3) Annealing at 1000 °C leads to a decrease in the intensity of almost all components; however, it significantly enhances Rt-Co.

The impact of increasing annealing time on φ_2=0°, 15°, 45°, and 65° sections of the ODFs of the FCC phase is presented in Fig. 11. Its comparison to Fig. 1(c) reveals that up to 30 min of annealing of the alloy at 900 °C does not affect the texture components strongly, and Brass, Rt-G, and S1 are the main texture components in the samples

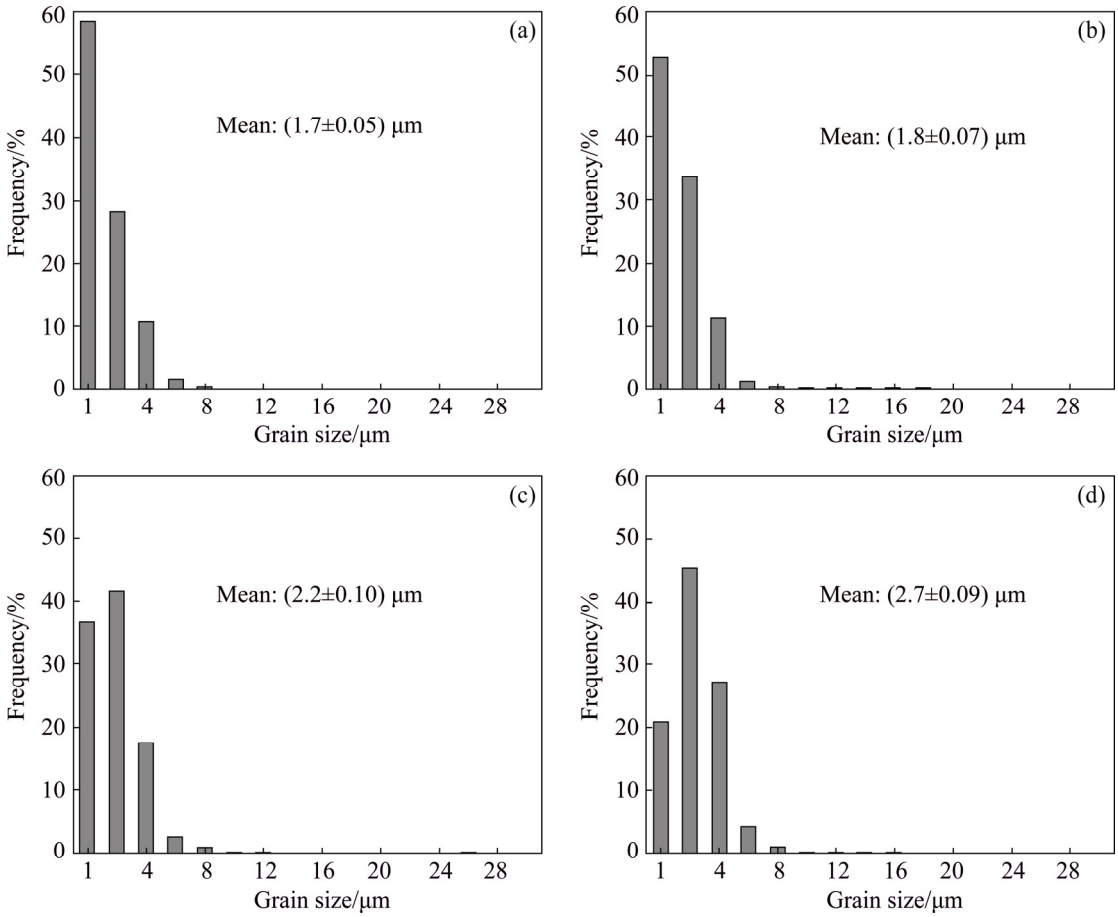

Fig. 9 Grain size distribution of samples annealed at 900 °C for 5 min (a), 30 min (b), 60 min (c) and 120 min (d)

annealed for 5 and 30 min at 900 °C. Increasing annealing time to 60 min led to the formation of a Cube texture component and weakening of the S1 component; nevertheless, Rt-G and brass remained almost stable. No change was seen in texture components by increasing time to 120 min; however, texture intensity decreased.

Table 4 reveals the maximum intensity of major texture components with increasing annealing time. It can be clearly seen that, by increasing annealing time, the intensity of S1 and Rt-G decreased; however, the intensity of the Cube, D, and Brass components increased. These variations intensify after 60 min of annealing. Furthermore, a slight reduction was observed in the intensity of all components after 120 min of annealing.

4 Discussion

FeCrCuMnNi HEA could be considered as an alloy with low to medium SFE [30], and it is known that softening behavior in heavily deformed, low SFE materials is characterized by the discontinuous recrystallization process that proceeds through the typical nucleation and grain growth stages [32]. Nucleation cites may be associated with pre-existing microstructural features, such as second phase particles or grain boundaries, or with inhomogeneities induced by deformation, such as shear bands and deformation bands [32]. As shown in Fig. 4(a), nucleation in FCC1 phase initiates at 600 °C. Figure 12 illustrates more precisely the microstructure of the sample. It can be seen in this figure that particle stimulated nucleation (PSN) occurs around the hard BCC particles. Generally, PSN has been observed in many alloys, including those of aluminium, iron, copper, and nickel, and is usually found to occur at particles with a diameter of greater than approximately 1 μm [32]. In most cases, a maximum of one grain is found to nucleate at any particle [32]; however, as can be seen in Fig. 12, here a significant number of nuclei formed around the BCC particle. Generally, second phase particles give rise to a high level of local lattice misorientation around the particle, in particle

Fig. 10 φ_2=0°, 15°, 45° and 65° sections of ODFs of FeCrCuMnNi HEA after annealing for 60 min at 600 °C (a), 700 °C (b), 800 °C (c), 900 °C (d) and 1000 °C (e)

Table 3 Maximum intensity of main texture components at different annealing temperatures

Texture component	600 °C	700 °C	800 °C	900 °C	1000 °C
Brass	2	4	1	6	0.5
Rt-G	7	9	7	3	4
S1	9	7	2	2	0.2
Cube	0.5	0.5	2	3	2
D	0	0	2	2	0.5
Rt-Co	0	0	0	0	10

deformation zone (PDZ), and during deformation. These can act as potent nucleation sites for new recrystallized grains; however, nucleation at a pre-existing subgrain within the deformation zone and nucleation through rapid sub-boundary migration are the main mechanisms during PSN [32]. Nevertheless, the formation of FCC1 nuclei in other parts of the sample is noticeable in this figure, which could be due to the grain boundaries or deformation heterogeneities. Nucleation of recrystallized FCC2 grains initiates at the temperature of 800 °C as shown in Figs. 4(c)

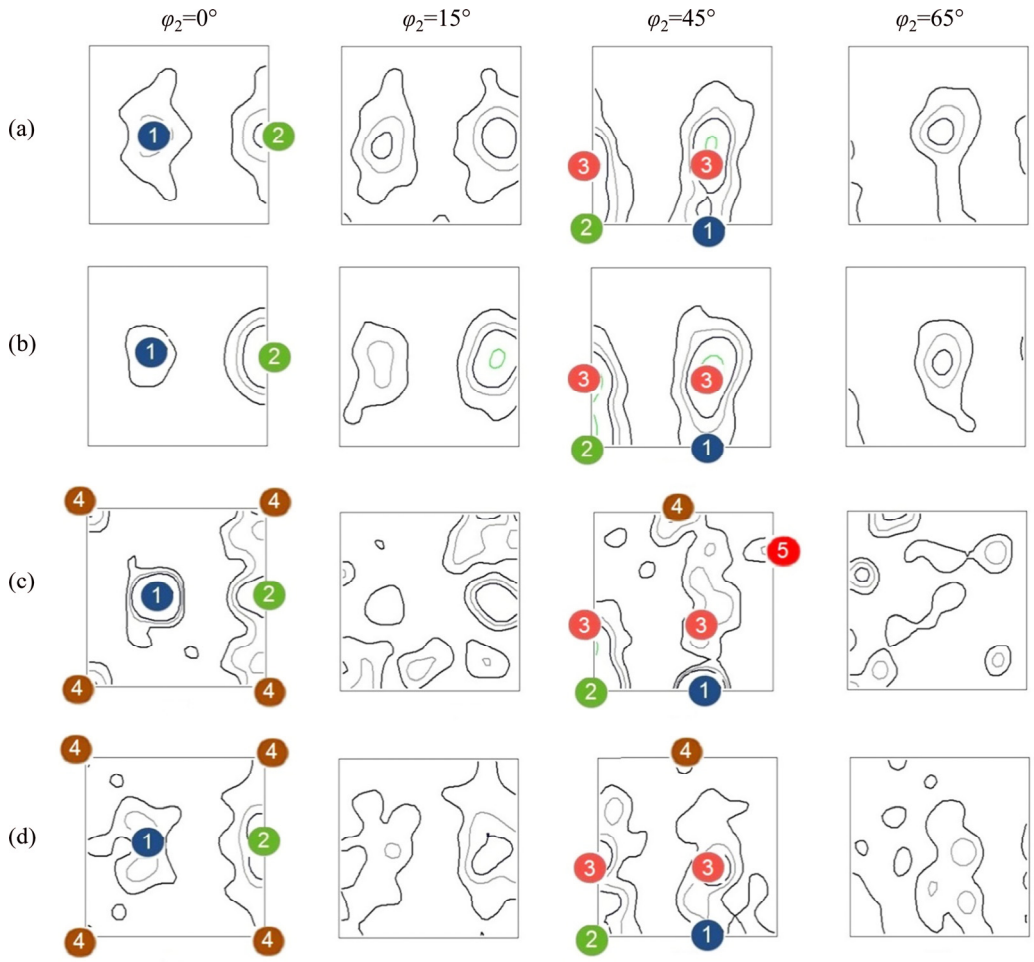

Fig. 11 φ_2=0°, 15°, 45°, and 65° sections of ODFs of FeCrCuMnNi HEA after annealing at 900 °C for 5 min (a), 30 min (b), 60 min (c) and 120 min (d)

Table 4 Maximum intensity of main texture components at different annealing time

Texture component	5 min	30 min	60 min	120 min
Brass	3	1	6	1
Rt-G	3	6	3	3
S1	6	6	2	3
Cube	0	0	3	1
D	0	0	2	0.5

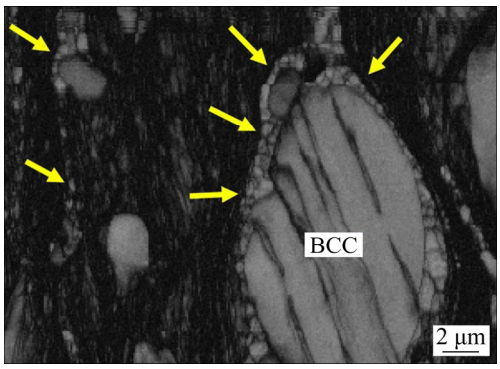

Fig. 12 SEM image of sample annealed at 600 °C for 60 min

and 13. It is evident that in spite of FCC1, in FCC2 a significant number of nuclei form in all parts of the phase. It can be concluded that FCC2 phase is less sensitive to PSN, and recrystallized grains form mostly at the grain boundaries or the inhomogeneities induced by the deformation. Formation of annealing twins is also evident in Fig. 13.

The results of the present study showed that mean grain size increased from 1.4 μm in the sample annealed at 600 °C for 60 min to 6.5 μm in the fully recrystallized sample annealed at 1000 °C. In addition, mean grain size increased from 1.8 μm in the sample annealed at 900 °C for 5 min to 2.7 μm in the sample annealed at 800 °C for 120 min. These results can be interpreted as evidence of a resistance to grain growth in the FeCrCuMnNi HEA. Furthermore, Figs. 4 and 7

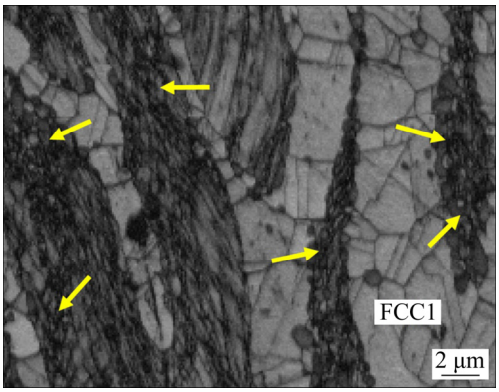

Fig. 13 SEM image of sample annealed at 800 °C for 60 min

reveal that a remarkable number of nuclei form during the annealing and the slow grain growth is the limiting parameter in the recrystallization of this alloy. Other recent studies have also shown low grain growth and fine-grained structure in different HEA systems [10−13,15,25]. Most researchers have reported the sluggish diffusion effect as the main reason for the low grain growth in HEAs [12,13, 15,25]. SATHIARAJ and BHATTACHARJEE [15] also asserted that the characteristics of the solute matrix reduce grain boundary movement, thus intensifying the sluggish grain growth behavior of the HEA. Theoretically, grain growth and grain boundary movement require dislocation slip [32]. TSAI et al [25] argued that solution hardening in HEAs inhibits the slip or cross-slip of dislocations. They also maintained that Suzuki's interaction in the whole-solute matrix significantly reduces the SFE and increases the spacing or stacking fault between paired Shockley partial dislocations, making cross-slip more difficult [25]. Nevertheless, it seems that the multi-phase characteristic of the alloy is also an effective parameter on low grain growth during annealing. Due to the distribution of the phases, the growth of one phase can be limited to the interface of the other phase. To our knowledge, there are not many investigations on the recrystallization of multiphase HEAs that have found large volume fractions of the phases. However, BAKER et al [13] pointed out that, in coarse two-phase alloys, one phase can limit the growth of the other phase.

Another point to be considered is the recrystallization order of the phases; FCC1 phase recrystallized in a shorter time and at a lower temperature as shown in Figs. 4 and 7. Using equation (2), the melting point of the phases can be roughly calculated [1]:

$$T_{\mathrm{m}} = \sum_{i=1}^{n} X_i (T_{\mathrm{m}})_i \tag{2}$$

where X_i is the mole fraction of component i and $(T_{\mathrm{m}})_i$ is the melting point of component i. The calculations reveal the melting points of 1233 and 1563 °C for the FCC1 and FCC2, respectively. The lower melting point of FCC1 could be a cause of the earlier recrystallization of this phase. However, the amount of deformation and strain can strongly affect recrystallization behavior. The stored energy, which provides the driving force for recrystallization, increases with strain. Therefore, both nucleation and growth are more rapid or occur at a lower temperature in a more highly deformed material [13,32]. SHABANI et al [30] recently reported that, in this HEA system, FCC1 phase deforms earlier during cold-rolling, and residual microstrain in FCC1 is almost 3 times greater than FCC2 phase after 85% reduction in thickness. Therefore, it can be concluded that lower melting point and higher residual microstrain are the main reasons for the earlier recrystallization of FCC1 phase.

As shown in Fig. 1(c), Brass, Rt-G, and S1 are the major texture components in FCC phase after deformation. The development of a strong brass texture during heavy cold-rolling is a behavior typically demonstrated by low SFE materials [30,33,34]. Tables 3 and 4 illustrate that the intensity of Rt-G and S1components decreases with increase in annealing temperature or time. Nevertheless, Cube and D components intensify. Brass reveals a variable behavior; however, it also seems to be a major component in the recrystallized sample. In the case of heavily cold-rolled, low to medium SFE, FCC metals and alloys, the recrystallization texture mostly consists of a strong Cube texture [12,32]. However, it has been reported that the recrystallization texture of these alloys is strongly influenced by initial grain size, annealing temperatures, imposed strain, and alloy composition [27,32]. It has been argued that the sharp Cube texture has its origin in either the preferred nucleation of grains with a particular orientation (oriented nucleation theory) or the preferred growth of grains of specific orientations

from a more randomly oriented array of nuclei (oriented growth theory) [32,35]. Therefore, the early recovery of the Cube regions can lead to the preferential nucleation of Cube grains and development of a strong Cube texture (oriented nucleation theory) [36], or the preferential growth of the Cube grains can be the main cause of the formation of the sharp Cube texture [12]. Nevertheless, small amounts of impurities can strongly decrease the Cube texture intensity [27,32]. This can be the main reason for the low intensity of the Cube texture in the recrystallized samples. However, the role of the sluggish diffusion effect in HEAs can be considered in this phenomenon, as the mobility of boundaries depends upon the diffusion in and across the grain boundaries. Therefore, sluggish diffusion can lead to smoother variations in texture intensities. Recent studies have shown almost the same variations in the texture of recrystallized HEAs [10,12,15,27]. As shown in Figs. 4, 7, and 12, annealing twins form in the alloy during recrystallization, especially in FCC1 phase. Formation of annealing twins is believed to be a key mechanism of texture evolution during recrystallization [16,32]. Based on a theory, annealing twins form due to migration of triple points, and new grains form during this migration, which leads to a decrease in total energy [37]. SATHIARAJ and BHATTACHARJEE [15] reported the formation of D and Copper textures during the recrystallization of HEAs. They argued that D and Copper texture components originate in the formation of annealing twins [15].

5 Conclusions

(1) No phase transformation was seen during annealing of the alloy with different annealing regimes.

(2) Due to its lower melting point and higher amount of deformation during cold-rolling, FCC1 phase recrystallized earlier than FCC2 phase.

(3) PSN seemed to be more effective on the recrystallization of FCC1 phase in which a large number of nuclei formed around the BCC particles at 600 °C.

(4) FCC1 phase fully recrystallized at 800 °C, when recrystallization initiated in FCC2 phase due to nucleation mostly at the grain boundaries and the inhomogeneities.

(5) Recrystallization led to the elimination of deformation texture components such as Rt-G and S1; however, annealing temperature seemed to be more effective on this elimination than annealing time.

(6) Increasing annealing temperature as well as annealing time led to the formation of Cube and D texture components; however, Brass texture also seemed to be a major component in recrystallized samples.

Acknowledgments

The financial support from the Iran National Science Foundation (INSF) through contract No. 97018809 is kindly appreciated.

References

[1] ZHANG Yong, ZUO Ting-ting, TANG Zhi, GAO M C, DAHMEN K A, LIAW P K, LU Zhao-ping, Microstructures and properties of high-entropy alloys [J]. Progress in Materials Science, 2014, 61: 1−93.

[2] WANG Pan, HUANG Peng-fei, NG F L, SIN W J, LU Sheng-lu, NAI M L S, DONG Zhi-li, WEI Jun. Additively manufactured CoCrFeNiMn high-entropy alloy via pre-alloyed powder [J]. Materials & Design, 2019, 168: 107576.

[3] SHAYSULTANOV D G, SALISHCHEV G A, IVANISENKO Y V, ZHEREBTSOV S V, TIKHONOVSKY M A, STEPANOV N D. Novel Fe36Mn21Cr18Ni15Al10 high entropy alloy with bcc/B2 dual-phase structure [J]. Journal of Alloys and Compounds, 2017, 705: 756−763.

[4] CHENG Hu, XIE Yan-chong, TANG Qun-hua, CONG Rao, DAI Pin-qiang. Microstructure and mechanical properties of FeCoCrNiMn high-entropy alloy produced by mechanical alloying and vacuum hot pressing sintering [J]. Transactions of Nonferrous Metals Society of China, 2018, 28: 1360−1367.

[5] ZHOU Shang-cheng, ZHANG Peng, XUE Yun-fei, WANG Fu-chi, LU WANG, CAO Tang-qing, ZHEN Tan, CHENG Bao-yuan, WANG Ben-peng. Microstructure evolution of Al0.6CoCrFeNi high entropy alloy powder prepared by high pressure gas atomization [J]. Transactions of Nonferrous Metals Society of China, 2018, 28: 939−945.

[6] KARATI A, GURUVIDYATHRI K, HARIHARAN V S, MURTY B S. Thermal stability of AlCoFeMnNi high-entropy alloy [J]. Scripta Materialia, 2019, 162: 465−467.

[7] CHOUDHURI D, GWALANI B, GORSSE S, KOMARASAMY M, MANTRI S A, SRINIVASAN S G, MISHRA R S, BANERJEE R. Enhancing strength and strain hardenability via deformation twinning in fcc-based high entropy alloys reinforced with intermetallic compounds [J]. Acta Materialia, 2019, 165: 420−430.

[8] CHEN Min-rui, LIN Su-jien, YEH Jien-wei, CHUANG Ming-hao, CHEN Swe-kai, HUANG Yuan-sheng. Effect of

vanadium addition on the microstructure, hardness, and wear resistance of Al0.5CoCrCuFeNi high-entropy alloy [J]. Metallurgical and Materials Transactions A, 2006, 37: 1363−1369.

[9] CHENG Jiang-bo, LIU Dan, LIANG Xiu-bing, XU Bin-shi. Microstructure and electrochemical properties of CoCrCuFeNiNb high-entropy alloys coatings [J]. Acta Metallurgica Sinica (English Letters), 2014, 27: 1031−1037.

[10] GUO Tong, LI Jin-shan, WANG Jun, WANG William-Yi, LIU Yi, LUO Xi-ming, KOU Hong-chao, BEAUGNON E. Microstructure and properties of bulk Al0.5CoCrFeNi high-entropy alloy by cold rolling and subsequent annealing [J]. Materials Science and Engineering A, 2018, 729: 141−148.

[11] WANI I S, BHATTACHARJEE T, SHEIKH S, CLARK I T, PARK M H, OKAWA T, GUO S, BHATTACHARJEE P P, TSUJI N. Cold-rolling and recrystallization textures of a nano-lamellar AlCoCrFeNi2.1 eutectic high entropy alloy [J]. Intermetallics, 2017, 84: 42−51.

[12] SATHIARAJ G D, AHMED M Z, BHATTACHARJEE P P. Microstructure and texture of heavily cold-rolled and annealed fcc equiatomic medium to high entropy alloys [J]. Journal of Alloys and Compounds, 2016, 664: 109−119.

[13] BAKER I, MENG F, WU M, BRANDENBERG A. Recrystallization of a novel two-phase FeNiMnAlCr high entropy alloy [J]. Journal of Alloys and Compounds, 2016, 656: 458−464.

[14] SHABANI A, TOROGHINEJAD M R, SHAFYEI A, LOGÉ R E. Evaluation of the mechanical properties of the heat treated FeCrCuMnNi high entropy alloy [J]. Materials Chemistry and Physics, 2019, 221: 68−77.

[15] SATHIARAJ G D, BHATTACHARJEE P P. Analysis of microstructure and microtexture during grain growth in low stacking fault energy equiatomic CoCrFeMnNi high entropy and Ni−60wt.%Co alloys [J]. Journal of Alloys and Compounds, 2015, 637: 267−276.

[16] SATHIARAJ G D, BHATTACHARJEE P P. Effect of starting grain size on the evolution of microstructure and texture during thermo-mechanical processing of CoCrFeMnNi high entropy alloy [J]. Journal of Alloys and Compounds, 2015, 647: 82−96.

[17] ZENG Z R, ZHU Y M, XU S W, BIAN M Z, DAVIES C H J, BIRBILIS N, NIE J F. Texture evolution during static recrystallization of cold-rolled magnesium alloys [J]. Acta Materialia, 2016, 105: 479−494.

[18] ODNOBOKOVA M, BELYAKOV A, ENIKEEV N, MOLODOV D A, KAIBYSHEV R. Annealing behavior of a 304L stainless steel processed by large strain cold and warm rolling [J]. Materials Science and Engineering A, 2017, 689: 370−383.

[19] FU Jian-xin, CAO Cheng-ming, WEI Tong, PENG Liang-ming. Effect of thermomechanical processing on microstructure and mechanical properties of CoCrFeNiMn high entropy alloy [J]. Transactions of Nonferrous Metals Society of China, 2018, 28: 931−938.

[20] BHATTACHARJEE T, WANI IS, SHEIKH S, CLARK IT, OKAWA T, GUO S, BHATTACHARJEE P P, TSUJI N. Simultaneous strength-ductility enhancement of a nano-lamellar AlCoCrFeNi2.1 eutectic high entropy alloy by cryo-rolling and annealing [J]. Scientific Reports, 2018, 8: 3276.

[21] SENKOV O N, PILCHAK A L, SEMIATIN S L. Effect of cold deformation and annealing on the microstructure and tensile properties of a HfNbTaTiZr refractory high entropy alloy [J]. Metallurgical and Materials Transactions A, 2018, 49: 2876−2892.

[22] ZHANG Cheng, ZHU Chao-yi, SHIN Su-min, VECCHIO K. Enhancement of ⟨001⟩ recrystallization texture in non-equiatomic Fe−Ni−Co−Al-based high entropy alloys by combination of annealing and Cr addition [J]. Journal of Alloys and Compounds, 2018, 768: 277−286.

[23] ANNASAMY M, HAGHDADI N, TAYLOR A, HODGSON P, FABIJANIC D. Dynamic recrystallization behaviour of $Al_xCoCrFeNi$ high entropy alloys during high-temperature plane strain compression [J]. Materials Science and Engineering A, 2019, 745: 90−106.

[24] SHABANI A, TOROGHINEJAD M R. Investigation of microstructure, texture, and mechanical properties of FeCrCuMnNi multiphase high entropy alloy during recrystallization [J]. Materials Characterization, 2019, 154: 253−263. DOI: https://doi.org/10.1016/j.matchar.2019.05.043.

[25] TSAI Che-wei, CHEN Yu-liang, TSAI Ming-hung, YEH Jien-wei, SHUN Tao-tsung, CHEN Swe-kai. Deformation and annealing behaviors of high-entropy alloy Al0.5 CoCrCuFeNi [J]. Journal of Alloys and Compounds, 2009, 486: 427−435.

[26] KLIMOVA M V, SHAYSULTANOV D G, CHERNICHENKO R S, SANIN V N, STEPANOV N D, ZHEREBTSOV S V, BELYAKOV A N. Recrystallized microstructures and mechanical properties of a C-containing CoCrFeNiMn-type high-entropy alloy [J]. Materials Science and Engineering A, 2019, 740: 201−210.

[27] BHATTACHARJEE P P, SATHIARAJ G D, ZAID M, GATTI J R, LEE Chi, TSAI Che-Wei, YEH Jien-Wei. Microstructure and texture evolution during annealing of equiatomic CoCrFeMnNi high-entropy alloy [J]. Journal of Alloys and Compounds, 2014, 587: 544−552.

[28] BHATTACHARJEE P P, JOSHI M, CHAUDHARY V P, ZAID M. The effect of starting grain size on the evolution of microstructure and texture in nickel during processing by cross-rolling [J]. Materials Characterization, 2013, 76: 21−27.

[29] SHABANI A, TOROGHINEJAD M R, SHAFYEI A, LOGÉ R E. Microstructure and mechanical properties of a multiphase FeCrCuMnNi high-entropy alloy [J]. Journal of Materials Engineering and Performance, 2019, 28: 2388−2398.

[30] SHABANI A, TOROGHINEJAD M R, SHAFYEI A, CAVALIERE P. Effect of cold-rolling on microstructure, texture and mechanical properties of an equiatomic FeCrCuMnNi high entropy alloy [J]. Materialia, 2018, 1: 175−184.

[31] REED-HILL R E, ABBASCHIAN R. Physical metallurgy principles [M]. Calif, USA: Brooks/Cole Engineering Division Monterey, 1973.

[32] HUMPHREYS F J, HATHERLY M, Recrystallization and related annealing phenomena [M]. 2ed, Amsterdam: Elsevier Ltd., 2004.

[33] HOU Jin-xiong, ZHANG Min, MA Sheng-guo, LIAW P K, ZHANG Yong, QIAO Jun-wei. Strengthening in Al0.25CoCrFeNi high-entropy alloys by cold rolling [J]. Materials Science and Engineering A, 2017, 707: 593−601.

[34] SHABANI A, TOROGHINEJAD M R. Study on texture evolution and shear behavior of an Al/Ni/Cu composite [J]. Journal of Materials Engineering and Performance, 2018, 27: 6004−6015.

[35] SADEGHI B, SHABANI A, CAVALIERE P. Hot rolling of spark-plasma-sintered pure aluminium [J]. Powder Metallurgy, 2018, 61: 285−292.

[36] DOHERTY R D. Recrystallization and texture [J]. Progress in Materials Science, 1997, 42: 39−58.

[37] FULLMAN R L, FISHER J C. Formation of annealing twins during grain growth [J]. Journal of Applied Physics, 1951, 22: 1350−1355.

冷轧 FeCrCuMnNi 多相高熵合金退火组织和织构形成的评价

Ali SHABANI, Mohammad Reza TOROGHINEJAD

Department of Materials Engineering, Isfahan University of Technology, Isfahan 84156-83111, Iran

摘　要：研究冷轧态 FeCrCuMnNi 多相高熵合金经不同退火处理后显微组织和织构的变化。样品经不同温度和不同时间热处理后进行不同的检测和表征，包括 X 射线衍射和扫描电镜−电子背散射衍射分析。结果显示，FCC1 相具有较低的熔点，再结晶温度较低，时间较短，且应变较大。此外，与 FCC2 相比较，粒子激发形核对 FCC1 相的再结晶更有效。在 BCC 颗粒周围形成了大量 FCC1 晶核。FCC2 的形核发生在 800 °C，大部分在晶界和不均匀处形核。此温度下，FCC1 相已经完全再结晶。退火过程导致轧制组织的消除，而再结晶样品中的主要成分仍然是黄铜。提高退火温度和延长退火时间导致立方织构的形成，立方织构是低堆垛层错能材料再结晶的主要成分。此外，由于退火孪晶的形成，再结晶过程中形成了 D 和 Rt-Co 成分。

关键词：高熵合金；FeCrCuMnNi；再结晶；显微组织；织构

(Edited by Xiang-qun LI)